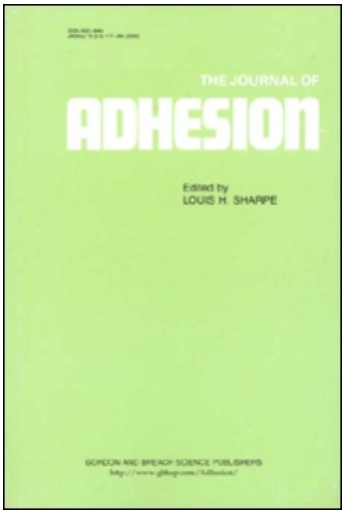

The Journal of Adhesion

Publication details, including instructions for authors and subscription information:
http://www.informaworld.com/smpp/title~content=t713453635

Measurement of Adhesion Between Carbon Fibers and Bismaleimide Resins

C. L. Heisey[a]; P. A. Wood[a]; J. E. McGrath[a]; J. P. Wightmany[a]
[a] Department of Chemistry, National Science Foundation Science & Technology Center: High Performance Polymeric Adhesives & Composites, and Center for Adhesive & Sealant Science, Virginia Polytechnic Institute & State University, Blacksburg, Virginia, USA

To cite this Article Heisey, C. L. , Wood, P. A. , McGrath, J. E. and Wightmany, J. P.(1995) 'Measurement of Adhesion Between Carbon Fibers and Bismaleimide Resins', The Journal of Adhesion, 53: 1, 117 — 147
To link to this Article: DOI: 10.1080/00218469508014375
URL: http://dx.doi.org/10.1080/00218469508014375

J. Adhesion, 1995, Vol. 53, pp. 117–147
Reprints available directly from the publisher
Photocopying permitted by license only

Measurement of Adhesion Between Carbon Fibers and Bismaleimide Resins*

C. L. HEISEY, P. A. WOOD, J. E. MCGRATH and J. P. WIGHTMAN**

Department of Chemistry, National Science Foundation Science & Technology Center: High Performance Polymeric Adhesives & Composites, and Center for Adhesive & Sealant Science, Virginia Polytechnic Institute & State University, Blacksburg, Virginia, USA

(Received July 18, 1994; in final form March 25, 1995)

The adhesion between carbon fibers and bismaleimide resins was evaluated using the microbond single fiber pull-out test. A commercially-available, methylene dianiline-based bismaleimide resin and a novel phosphorus-containing bismaleimide were tested with as-received and plasma-treated polyacrylonitrile-based carbon fibers. The surface chemical composition, topography, tensile strength, and surface free energy of the carbon fibers were studied using x-ray photoelectron spectroscopy, scanning electron microscopy, single fiber tensile tests, and dynamic contact angle analysis. The carbon fiber-bismaleimide adhesion improved when the carbon fiber received an oxidative commercial surface treatment or was exposed to an air or ammonia plasma prior to bonding.

KEYWORDS: bismaleimide; fiber-matrix adhesion; glow discharge plasma; microbond pull-out test; surface free energy; x-ray photoelectron spectroscopy

INTRODUCTION

The degree of adhesion between the fibers and the matrix and the nature of the fiber-matrix interphase have a major influence on the mechanical properties of a composite.[1,2] "Good" fiber-matrix adhesion is required for efficient transfer of stress from the matrix to the reinforcing fibers. Fiber-matrix adhesion is generally attributed to chemical, physical, and/or mechanical bonding at the fiber-matrix interface.

A number of tests have been developed to determine the capacity of the interface to transfer stress from the matrix to the fiber(s) in real composites and in model single fiber composites.[3] Single fiber fragmentation,[4–19] indentation,[1,20–22] microbond,[1,19,23–31] fiber pull-out from a resin block,[32–36] fiber pull-out from a microcomposite,[37] laser Raman spectroscopy,[38] a three-fiber pull-out technique,[39] and mechanical tests such as the short beam shear test, Iosipescu shear test, and transverse and off-axis tensile tests[1,40–45] have been used to evaluate fiber-matrix adhesion. Each of these methods has inherent problems that limit its application as a universal test method.[23]

Traditionally, epoxies have been the major resins chosen for use as composite matrices and adhesives. Therefore, the majority of fiber-matrix adhesion studies have

*One of a Collection of papers honoring Lawrence T. Drzal, the recipient in February 1994 of *The Adhesion Society Award for Excellence in Adhesion Science*, Sponsored by 3M.

** Corresponding author.

involved carbon fibers and epoxy resins.[4-11, 21, 23] Bismaleimides, a type of thermosetting polyimide, are preferred over epoxies in applications where high temperature resistance, good hot-wet environmental stability and improved fire and smoke properties are required.[46] However, relatively few studies are reported in the literature involving carbon fiber-bismaleimide adhesion. Bismaleimides are low molecular weight monomers or prepolymers which have imide moities in the backbone structure and are terminated by reactive groups which polymerize by thermal or catalytic means.[47] Bismaleimide resins process in a manner similar to epoxies, cure without the evolution of by-products, and exhibit a balance of thermal and mechanical properties which make them popular for use in advanced composites, structural adhesives, and in electronic applications.[47, 48]

The adhesion of bismaleimide resins to carbon fibers has been studied by measuring the properties of carbon fiber-reinforced bismaleimide composites. Jang prepared composites using Ciba-Geigy's Matrimid® 5292 bismaleimide resin and either as-received or plasma-treated AU-4 carbon fibers.[49] Exposing the carbon fibers to either argon, air, or ammonia plasmas improved the transverse strength of the composites. Wilkinson blended poly (ethersulfone) with the Matrimid 5292 bismaleimide resin and prepared AU-4 and AS-4 carbon fiber-reinforced composites.[50] Micro-and meso-indentation tests showed that the bismaleimide-poly (ethersulfone) blend adhered better to the surface-treated AS-4 carbon fiber than to the untreated AU-4 carbon fiber.

Allred and Harrah measured the transverse tensile and transverse flexure strength of carbon fiber-reinforced bismaleimide composites.[51] The bismaleimide adhesion improved when the carbon fibers were exposed to an acidic plasma and the failure mode was shifted from interfacial for the untreated fibers to cohesive within the bismaleimide for the plasma-treated fibers. Lee and Holguin developed a modified single fiber fragmentation test for use with highly cross-linked brittle bismaleimide matrices; however, the effect of fiber surface treatment on the carbon fiber-bismaleimide adhesion was not investigated.[52]

In this study, the adhesion of two different bismaleimide resins to as-received and plasma-treated carbon fibers was evaluated using the microbond single fiber pull-out test. The microbond test was chosen due to the relative ease of sample preparation and the small amount of resin required to prepare the bismaleimide microdroplets. The small amount of resin required in the microbond test is a distinct advantage when working with novel polymers which are available in limited quantity.

EXPERIMENTAL

I Materials

Hercules AU-4 and AS-4 polyacrylonitrile-based, high-strength, low-modulus carbon fibers were used in this study. The AS-4 carbon fiber received a proprietary surface treatment as part of production. The AU-4 carbon fiber was not surface treated. The carbon fibers were received without sizing in a tow containing 12,000 continuous filaments and were used "as received".

The Matrimid® 5292 A/B thermosetting bismaleimide resin system was supplied by Ciba-Geigy. The chemical structures of the two components of the Matrimid A/B

4,4'-bismaleimidodiphenyl methane

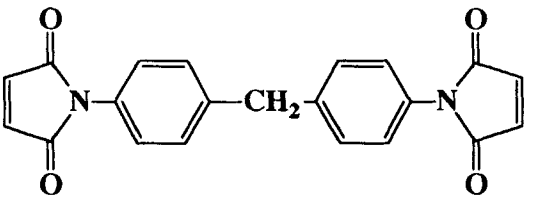

o,o'-diallyl bisphenol A (DABA)

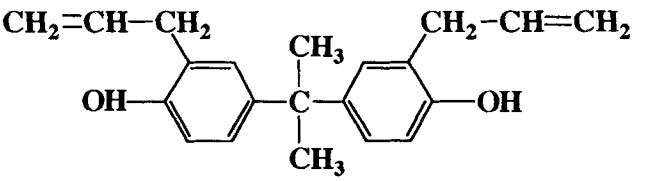

FIGURE 1 Matrimid® 5292 A/B thermosetting resin system.

bismaleimide resin system are shown in Figure 1. Part A is 4,4'-bismaleimidodiphenyl methane, the common bismaleimide based on methylene dianiline. Part B is *o, o'*-diallyl bisphenol A (DABA), a reactive diluent which improves the processing window of the bismaleimide. Improvement in the processing window is required since this methylene dianiline-based bismaleimide normally reacts and gels just a few degrees above its 140°C melting point. The ratio of DABA to bismaleimide was held constant at 1.0 mole bismaleimide to 0.85 mole of DABA (57:43 parts by weight).

The *bis* (3-maleimido phenoxy) triphenylphosphine oxide (BMPPO), in Figure 2, was synthesized by Wood and coworkers and characterized using ^{1}H-NMR and ^{13}C-NMR solution measurements, Fourier transform infrared spectroscopy, and bismaleic acid titration to ensure that the intended structure was obtained.[53] The BMPPO bismaleimide melts at 92°C and cures at temperatures exceeding 180°C. Therefore, unlike the methylene dianiline-based bismaleimides which begin to cure almost immediately upon melting, the BMPPO bismaleimide has a practical

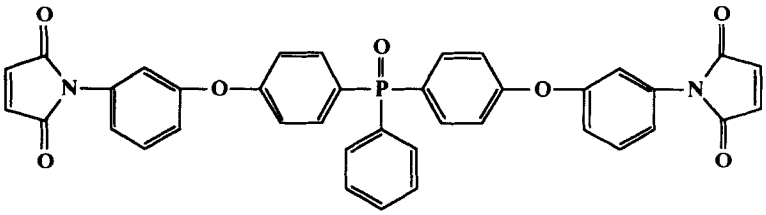

FIGURE 2 Chemical structure of *bis*(3-maleimido phenoxy) triphenylphosphine oxide (BMPPO).

processing window. The incorporation of phosphine oxide into polymers has been shown to impart flame retardancy, increase resistance to atomic oxygen, and improve adhesion of the polymer to metals.[54–56]

II Plasma Treatment

A March solid state Plasmod® was used to produce radiofrequency (13.56 MHz)-generated 50-watt glow discharge plasmas of air, oxygen, and ammonia. A March GCM-200 Gas Control Module regulated the chamber pressure to 1 torr. The barrel-shaped sample reactor was made of quartz. The ammonia gas was obtained from Matheson Gas Products (99.999%) and the oxygen gas was obtained from Airco, Inc. (99.95%). Room air was used for the air plasma treatment.

III X-ray Photoelectron Spectroscopy (XPS)

XPS was used to determine the elemental surface composition of the as-received AU-4 and AS-4 carbon fibers and to characterize the changes in the fiber surface chemistry following plasma treatment. The carbon fiber tows were analyzed using a Perkin-Elmer PHI 5400 x-ray photoelectron spectrometer with a Mg K_α x-ray source (1253.6 eV) operated at 15 kV and 400 watts with an emission current of 30 mA. The spectrometer was calibrated to the gold $4f_{7/2}$, copper $2p_{3/2}$, and silver $3d_{5/2}$ photopeaks according to the Perkin-Elmer standard procedure. Pressure inside the spectrometer sample chamber was held below 5×10^{-7} torr during analysis.

The carbon fiber tows were introduced into the spectrometer on an aluminum mount machined for use with fibers. A single fiber tow was placed on the mount and an aluminum ring was placed on top of the tow, covering the fiber ends. The aluminum ring was then secured on the aluminum mount with two screws. The area of the sample which was analyzed was approximately 1 mm × 3 mm in size.

Survey scans were taken in the range of 0–1100 eV and narrow scans were obtained on any significant peaks observed in the survey spectra. The binding energy of each photopeak was referenced to the carbon 1s photopeak at 284.6 eV. The binding energy of the carbon 1s photopeak was determined by sputtering the samples with gold and referencing the carbon 1s photopeak to the gold $4f_{7/2}$ photopeak at 83.8 eV. The PHI software (version 4.0) was used to obtain peak areas, calculate atomic concentrations, and to fit the photopeaks with Gaussian-Lorentzian curves. The carbon 1s photopeaks were fit with $80 \pm 10\%$ Gaussian curves, varying the peak intensity and binding energy while holding the full width at half maximum (FWHM) at 1.4 ± 0.1 eV.

The XPS sampling depth was varied by tilting the sample by an angle (θ) with respect to the analyser. The relationship between the XPS sampling depth (d) and the take-off angle (θ) is defined by Equation (1),

$$d = 3\lambda \sin\theta \tag{1}$$

where λ is the electron inelastic mean free path. The long axis of the carbon fibers was aligned parallel with that of the analyser so that the analyser was effectively "seeing" a flat surface.[57] Spectra were obtained at take-off angles of 15°, 45° and 90°.

IV Scanning Electron Microscopy (SEM)

An ISI-SX-40 scanning electron microscope, operated at an acceleration voltage of 10 kV, was used to take photomicrographs of the microbond pull-out samples. The microbond pull-out samples were secured on aluminum mounts using silver paint and sputter-coated with gold using an Edwards Sputter Coater S150 B. A Philips EM-420T scanning transmission electron microscope, operated at an acceleration voltage of 60 kV, was used to take photomicrographs of the as-received and plasma-treated carbon fibers. The carbon fibers were secured on copper mounts using silver paint and coated with gold using a Polaron high resolution sputter coater.

V Dynamic Contact Angle Analysis

Individual carbon fibers were separated from the carbon fiber tow and mounted to the end of a 100 μm diameter copper wire hook with a cyanoacrylate adhesive. The fibers were carefully cut and handled to avoid damage or contamination. A fiber specimen was suspended by the wire hook from the arm of a CAHN dynamic contact angle system microbalance. A 10 ml glass beaker containing the liquid to be used for the contact angle measurement was raised to the fiber tip at a speed of 20 μm per second.

Upon contact of the carbon fiber with the liquid, the balance registered a wetting force (F) given by Equation (2),

$$F = \pi d \gamma_{LV} \cos\theta - B \tag{2}$$

where γ_{LV} is the surface free energy of the wetting liquid, θ is the contact angle, πd is the perimeter of the fiber at the liquid/solid interface, and B is the effect of buoyancy. When using small diameter carbon fibers, the effect of buoyancy is negligible and the contact angle is given by Equation (3).

$$\theta = \cos^{-1}\left[\frac{F}{\pi d \gamma_{LV}}\right] \tag{3}$$

The advancing contact angle was calculated using the average force measured as approximately 3 mm of the fiber was immersed in the wetting liquid and the receding contact angle was calculated using the average force measured as the fiber was removed from the liquid. Each fiber was contacted one time with only one liquid to avoid cross contamination or changes in the fiber surface chemistry.

The diameters of the carbon fibers, determined using dynamic contact angle analysis with *n*-hexane, are listed in Table I. It was assumed that *n*-hexane formed a 0° contact angle with the carbon fibers. When $\theta = 0°$, Equation (3) can be rearranged to define the fiber diameter as,

$$d = \frac{F}{\pi \gamma_{LV} \cos\theta} = \frac{F}{\pi \gamma_{LV}} \tag{4}$$

where γ_{LV} of *n*-hexane at 25°C is 18.6 mJ/m^2. The diameters determined by wetting analysis corresponds well with the respective diameters measured using scanning electron microscopy (10,000 X magnification). This argument supports the assumption that *n*-hexane formed a 0° contact angle with the carbon fibers.

TABLE I
Diameter of the as-received and plasma-treated carbon fibers determined using dynamic contact angle analysis with *n*-hexane

Carbon Fiber	$\langle$Diameter$\rangle \pm \sigma_{n-1}$ ($n = 15$) (μm)
as-received AU-4	6.5 ± 0.2
as-received AS-4	6.8 ± 0.6
15-sec. air-plasma-treated AS-4	6.7 ± 0.3
1-min. NH_3-plasma-treated AS-4	7.2 ± 0.4

The surface free energies of the liquids used in the dynamic contact angle experiments are listed in Table II. The total surface free energy of each liquid was determined using the Wilhelmy slide method.[58] The dispersive contribution to the total surface free energy of each liquid was obtained using the relationship proposed by Fowkes.[59] It was then assumed that the total surface free energy (γ_L) of the liquids was equal to the sum of the dispersive (γ_L^d) and the polar (γ_L^p) components as given in Equation (5).

$$\gamma_L = \gamma_L^d + \gamma_L^p \tag{5}$$

The polar component of the total surface free energy of the liquid was obtained by subtracting the dispersive component from the total surface free energy.

The surface free energies of the carbon fibers were determined using the one-liquid and the two-liquid wetting techniques depicted schematically in Figure 3. In the one-liquid approach of Owens and Wendt[60] and Dynes and Kaelble,[61, 62] the carbon fibers were wet with a variety of liquids with known polar and dispersive surface free energies and the liquid/carbon fiber contact angles were measured. The liquids used in the analysis were deionized water, formamide, diiodomethane, and bromonaphthalene. Based on Equation (6), the dispersive (γ_S^d) and the polar surface free energy components (γ_S^p) of the carbon fibers were determined from the intercept and the slope, respectively, of a line fit to a plot of $[\gamma_L(1 + \cos\theta)]/2\sqrt{\gamma_L^d}$ *versus* $\sqrt{\gamma_L^p/\gamma_L^d}$ using linear regression analysis.

$$\gamma_L(1 + \cos\theta) = 2\sqrt{\gamma_S^d\gamma_L^d} + 2\sqrt{\gamma_S^p\gamma_L^p} \tag{6}$$

TABLE II
Surface free energies of liquids used in dynamic contact angle analysis

Liquid	γ_L (mJ/m^2)	γ_L^p (mJ/m^2)	γ_L^d (mJ/m^2)
deionized water	72.7	49.2	23.5
formamide	58.3	25.3	33.0
diiodomethane	50.8	2.4	48.4
bromonaphthalene	44.6	0	44.6
n-hexane	18.6	0	18.6
n-octane	21.5	0	21.5
n-decane	23.8	0	23.8
n-hexadecane	27.8	0	27.8
decahydronaphthalene	31.8	0	31.8

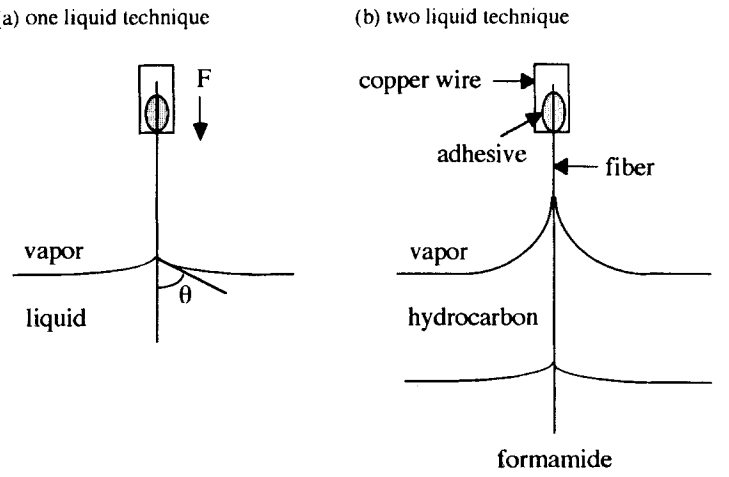

FIGURE 3 Schematic illustrations of (a) one-liquid and (b) two-liquid wetting force measurements.

The total surface free energy (γ_S) of the carbon fibers was obtained by summing the polar and the dispersive components.

In the two-liquid technique, the fiber was immersed in a 10 ml beaker containing two immiscible liquids: formamide and a hydrocarbon.[63, 64] The hydrocarbon liquids used in the analysis were *n*-hexane, *n*-octane, *n*-decane, *n*-hexadecane, and decahydronaphthalene. Based on Equation (7), $\gamma_F - \gamma_H + \tau$ was calculated and plotted *versus* $[\sqrt{\gamma_F^d} - \sqrt{\gamma_H}]$.

$$\gamma_F - \gamma_H + \tau = 2\sqrt{\gamma_S^d}\left[\sqrt{\gamma_F^d} - \sqrt{\gamma_H}\right] + I_{S/F}^p \tag{7}$$

In Equation 7, γ_F and γ_F^d are the total surface free energy and the dispersive component of the surface free energy of formamide, γ_H is the surface tension of the hydrocarbon, and $I_{S/F}^p$ is the polar interaction parameter. τ is defined in Equation 8,

$$\tau = \gamma_{F/H}\cos\theta_{S/F/H} = \frac{F - F_H}{\pi d} \tag{8}$$

where $\theta_{S/F/H}$ is the contact angle at the triple-phase line, $\gamma_{F/H}$ is the interfacial free energy between formamide and the hydrocarbon, πd is the fiber perimeter, F_H is the force recorded by the balance when the fiber is immersed in the hydrocarbon layer, and F is the total force recorded by the balance when the fiber has passed through the hydrocarbon layer and entered the formamide.

A line was fit to the data points using linear regression and the dispersive surface free energy component (γ_S^d) and the polar interaction parameter ($I_{S/F}^p$) of the carbon fibers were obtained from the slope and the intercept of the line, respectively. The polar component to the carbon fiber surface free energy was obtained using Equation (9) in which the assumption is made that the polar interaction term is equal to twice the geometric mean of the polar components.[65]

$$I_{S/F}^p = 2\sqrt{\gamma_S^p \gamma_L^p} \tag{9}$$

Note that Fowkes stated that Equation (9) is incorrect and that the polar interaction term is due to acid-base interactions.[66] The total surface free energy of the carbon fibers was obtained by adding the polar and the dispersive surface free energy components.

VII Tensile Strength

A single carbon fiber was separated from the tow and mounted between two aluminum tabs connected with two thin paper strips and epoxy adhesive. The fiber long axis was carefully aligned in the tensile direction. The fiber was affixed to the aluminum tabs using an epoxy adhesive and the epoxy was allowed to cure for 8 hours at room temperature as specified by the epoxy manufacturer.

A metal hook was hung from the bottom of a Mettler PM300 balance. The fiber tensile specimen was suspended from the hook by the hole-punched aluminum tab. The lower tab was secured between the blades of a custom-built miniature vise mounted on an elevator. Once the tensile specimen was secured in the vise, portions of both paper strips were burned away using a soldering iron and only the carbon fiber was left suspended between the aluminum tabs. The elevator was lowered at a rate of 5 μm per second and the load applied to the fiber was recorded as a function of time with a personal computer. The carbon fiber tensile strength data was analyzed using the Weibull distribution.[67]

VIII Microbond Pull-Out Test

To form a microbond test specimen, one end of a 4 cm long carbon fiber was affixed to a hole-punched aluminum tab using 3M Scotch™ glass cloth electrical tape. The metal tab was attached with a screw to one side of an aluminum frame. The central 2.5 cm of the fiber was suspended horizontally over open space and the free end of the carbon fiber was affixed to the far end of the aluminum frame using another small square of electrical tape.

To prepare the Matrimid 5292 droplets, the diallyl of bisphenol A (DABA) was weighed into a clean round bottom flask. A PTFE-coated magnetic stir bar was placed in the flask and the flask was lowered into a 130°C silicone oil bath. The temperature of the oil bath was increased to 140°C and the bismaleimide resin was added using a powder funnel. The resin was stirred for approximately 20 minutes. A dark reddish brown homogeneous hot-melt solution was obtained. The BMPPO bismaleimide powder was simply heated to melt on a hot plate in an aluminum pan.

Very long, thin strands of the bismaleimide resin were pulled out of the container of molten bismaleimide with a small diameter copper wire. This bismaleimide strand was placed perpendicular to the carbon fiber and a soldering iron was used to melt the strand of bismaleimide down around the fiber forming an axisymmetric droplet of bismaleimide on the fiber. The soldering iron was not brought into direct contact with the bismaleimide, but simply used to heat the air directly around the bismaleimide. The maximum temperature recorded by a thermocouple just in front of, but not touching, the soldering iron tip was 140°C. Thirteen microbond test specimens were prepared simultaneously on the metal frame.

The Matrimid bismaleimide droplets were heated on the carbon fibers at 130°C for 2 hours in a vacuum oven to degas the resin and then cured in a convection oven at 200°C

for 1 hour and 250°C for 2 hours. The BMPPO bismaleimide droplets were heated on the carbon fibers at 130°C for 1.5 hours in a vacuum oven to degas the resin and then cured in a convection oven at 225°C for 3.5 hours and at 300°C for 3 hours. Following the bismaleimide cure cycle, the carbon fibers were bonded to the aluminum tabs using an epoxy adhesive. The epoxy adhesive was cured overnight at room temperature as specified by the epoxy manufacturer.

The length of the fiber embedded in each cured bismaleimide droplet was measured using a Nikon-UM2 Measurescope. Void-free, axisymmetric bismaleimide droplets with embedded lengths ranging from 40 to 200 μm were successfully cured around single carbon fibers. Figure 4 is a scanning electron photomicrograph of a typical bismaleimide droplet cured around a carbon fiber.

The microbond test was used to measure the load required to debond the cured bismaleimide droplets from the carbon fibers. Figure 5 is a schematic illustration of the microbond test set-up. The fiber was suspended by a metal hook from a Mettler PM 300 balance. The samples were tested in shear using a custom-made miniature vise. The shearing plates were closed to a distance just greater than the fiber diameter with the aid of a video camera and monitor. The microvise was fixed on a motorized stage that moved downward at a rate of 5 μm per second. The data were transmitted from the balance to a personal computer at a rate of 6 data points per second.

RESULTS AND DISCUSSION

I Surface Chemical Composition

Carbon, oxygen, and nitrogen were detected on the AU-4 carbon fiber surface using XPS. Carbon, oxygen, and nitrogen, as well as sodium, were detected on the as-received

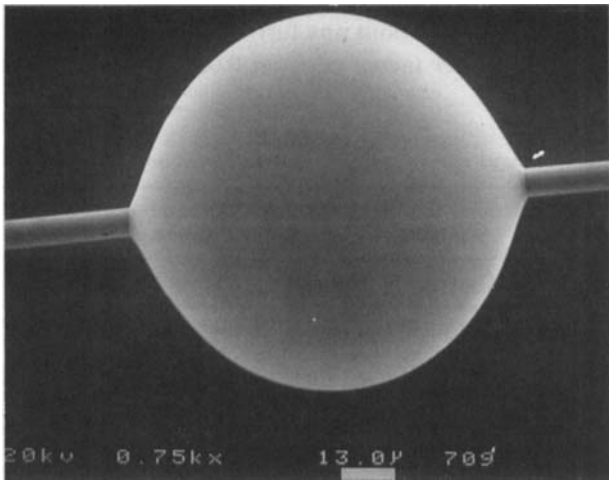

FIGURE 4 SEM photomicrograph of a BMPPO bismaleimide droplet cured around an AS-4 carbon fiber (750X).

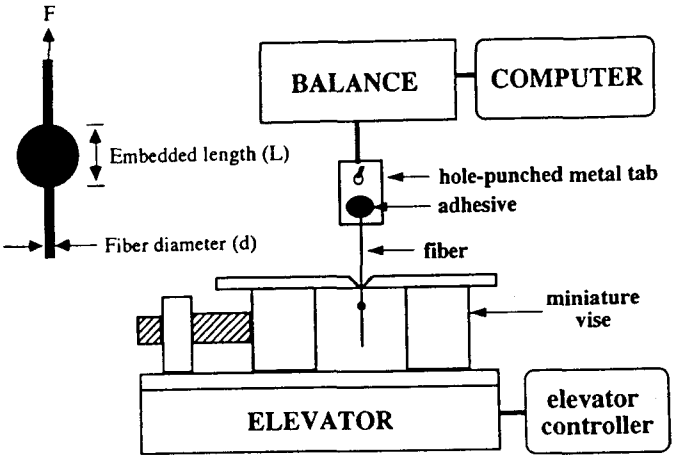

FIGURE 5 Schematic illustration of the microbond single fiber pull-out test.

and plasma-treated AS-4 carbon fibers. The concentration of each element detected on the carbon fiber surfaces is listed in Table III. There was more oxygen on the surface of the AS-4 carbon fiber than on the AU-4 carbon fiber as a result of the oxidative surface treatment that the AS-4 carbon fiber received during production. The sodium present on the AS-4 carbon fiber is probably a residual impurity from the sodium alkyl sulfonate added to the polyacrylonitrile carbon fiber precursor material.[68]

The O/C, N/C, and Na/C ratios of the AS-4 carbon fiber surface are plotted in Figures 6, 7 and 8, respectively, as a function of plasma exposure time. The air plasma treatment increased the O/C ratio of the AS-4 fiber surface from 0.11 to 0.27 in only 15 seconds, while the ammonia plasma decreased the O/C ratio from 0.11 to 0.086 in approximately 30 seconds. Additional exposure, for up to 5 minutes, in either the air or ammonia plasma did not bring about any further change in the O/C ratio. The N/C ratio of the AS-4 carbon fiber increased from 0.031 to 0.050 following a 1 minute

TABLE III
Surface composition of the as-received and plasma-treated carbon fibers (XPS, 45° take-off angle)

FIBER	CONCENTRATION ($\langle$atomic %$\rangle \pm \sigma_{n-1}$ for 3 samples)				ATOMIC RATIO		
	Carbon	Oxygen	Nitrogen	Sodium	O/C	N/C	Na/C
as-received AU-4	91.9 ± 0.9	6.0 ± 0.8	2.1 ± 0.2	nsp*	0.065	0.022	nsp
as-received AS-4	87.8 ± 1.2	9.3 ± 1.0	2.7 ± 0.1	0.2 ± 0.1	0.11	0.031	0.003
15-sec. air plasma AS-4	76.3 ± 0.7	19.8 ± 0.8	3.3 ± 0.2	0.6 ± 0.3	0.28	0.043	0.007
1-min. NH_3 plasma AS-4	86.8 ± 2.2	7.5 ± 1.4	5.2 ± 0.8	0.5 ± 0.1	0.086	0.060	0.005

* no significant peak

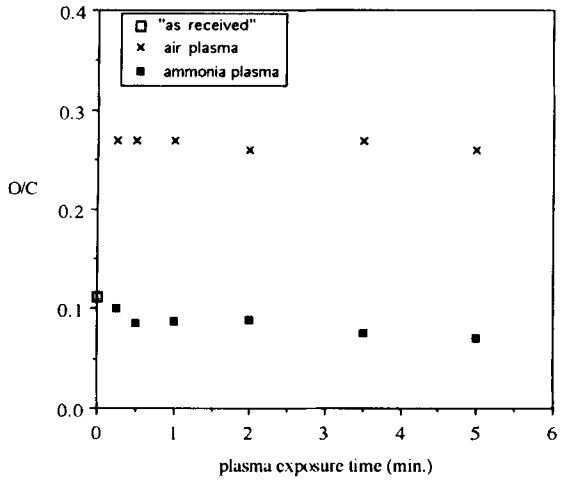

FIGURE 6 AS-4 carbon fiber O/C ratio as a function of plasma exposure time (XPS, 45° take-off angle).

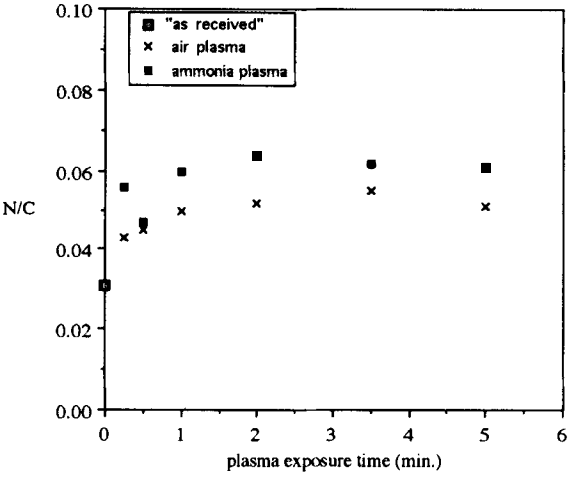

FIGURE 7 AS-4 carbon fiber N/C ratio as a function of plasma exposure time (XPS, 45° take-off angle).

air-plasma treatment and from 0.031 to 0.060 with a 1 minute ammonia-plasma treatment. As with the O/C ratio, additional air or ammonia plasma exposure did not bring about any further change in the N/C ratio.

The N/C and the O/C ratios of the air and ammonia plasma-treated carbon fiber surfaces became independent of plasma treatment time once the active sites on the fiber surface were saturated or a steady state condition was established in which the rate of incorporation of functional groups was equivalent to the rate of removal of the

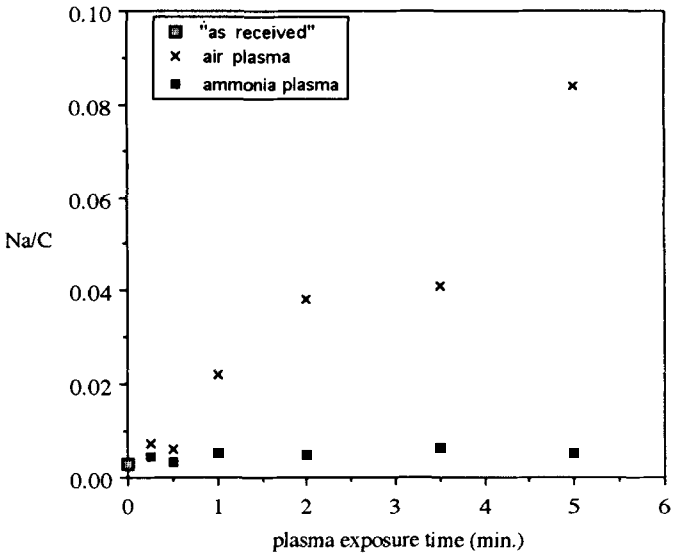

FIGURE 8 AS-4 carbon fiber Na/C ratio as a function of plasma exposure time (XPS, 45° take-off angle).

functional groups by further oxidation. Jones and Sammann also reported that prolonged exposure of carbon fibers to an air plasma (from 30 seconds to 30 minutes) did not change the fiber surface oxygen concentration.[69]

The air-plasma treatment increased the Na/C ratio from 0.0026 to 0.0074 in 15 seconds and the ratio continued to increase with exposure time. The Na/C ratio reached 0.084 following a 5-minute air-plasma treatment. The air plasma ablated the carbon fiber surface as the organic portion of the carbon fiber surface was oxidized into volatile species. The sodium in the carbon fiber surface was not removed as a volatile specie. Therefore, as the organic portion of the fiber surface was etched away, the surface became enriched with sodium. The ammonia plasma increased the Na/C ratio of the AS-4 carbon fibers from 0.0026 to 0.0053 in 1 minute, after which the Na/C ratio remained relatively constant. The fact that the Na/C ratio of the AS-4 carbon fiber surface did not increase as significantly in the ammonia plasma as in the air plasma, suggests that the ammonia plasma was not nearly as ablative as the air-plasma treatment.

The carbon 1s photopeak of the carbon fibers exhibited a pronounced asymmetric tailing toward higher binding energy values. This tail arose partly from the intrinsic asymmetry of the graphitic carbon peak and partly from peaks arising from oxygen and nitrogen-containing functional groups.[70, 71] In this study, the carbon 1s photopeak of the carbon fibers was fit with six peaks as shown in Figure 9. The carbon 1s peak assignments were made based on the work of Beamson and Briggs,[72] Desimoni *et al.*,[70, 71] and Sherwood and coworkers.[73-77]

The first peak was fit at 284.6 eV and was assigned to graphitic and aliphatic carbon-to-carbon bonding. The second peak was fit at 285.9 eV and was assigned to

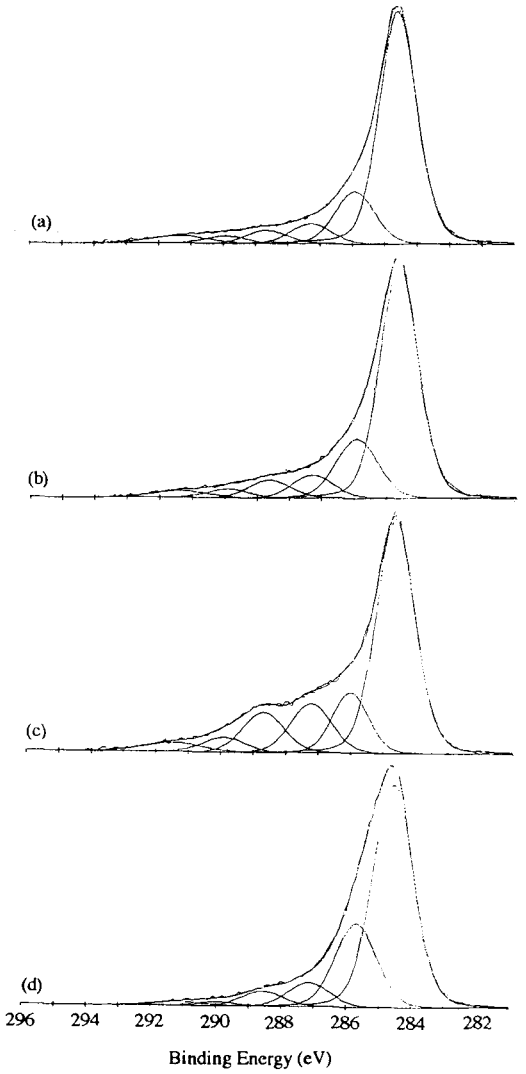

FIGURE 9 Curve-fit carbon 1s photopeak for (a) as-received AU-4, (b) as-received AS-4, (c) 15-sec. air-plasma-treated AS-4, and (d) 1-min. ammonia-plasma- treated AS-4 carbon fibers.

carbon singly-bonded to oxygen and to carbon bonded to nitrogen. The third peak was fit at 287.3 eV and was assigned to carbonyl and N—C = O groups. The fourth peak was fit at 288.7 eV and was assigned to carboxylic groups. The fifth peak was fit at about 289.9 eV and was attributed to carbonate groups and to adsorbed CO_2. A plasmon loss peak was fit at 291.3 eV as described by Proctor and Sherwood.[74] The contributions of each carbon 1s curve-fit peak for the as-received and plasma-treated carbon fibers, expressed in percent of the total composition, are summarized in Table IV.

TABLE IV
Carbon 1s curve-fitting results for the as-received and plasma-treated carbon fibers

FIBER	⟨% of Total Carbon 1s Peak Area⟩ $\pm \sigma_{n-1}$ for 3 samples					
	Binding Energy (eV)*					
	284.6	285.9	287.3	288.7	289.9	291.3
as-received AU-4	68.8 ± 0.1	14.1 ± 1.9	6.3 ± 0.3	4.1 ± 0.1	2.9 ± 0.8	3.8 ± 0.6
as-received AS-4	65.5 ± 0.2	16.7 ± 0.8	6.8 ± 0.2	5.5 ± 0.3	2.7 ± 0.1	2.8 ± 0.3
15-sec. air plasma AS-4	55.4 ± 0.4	13.9 ± 1.5	11.9 ± 1.0	9.9 ± 1.0	5.1 ± 0.3	3.8 ± 0.2
1-min. NH_3 plasma AS-4	61.4 ± 3.7	22.9 ± 2.0	7.3 ± 0.9	5.0 ± 0.9	1.6 ± 0.4	1.8 ± 0.3
ORIGIN	C—H_x	C—OH C—O—C C—N C = N	C = O N—C = O	O = C—OH O = C—OR	O—CO—O O = C—O— O = C = O	plasmon loss
PEAK NO.	1	2	3	4	5	6

* Uncertainty in carbon 1s contributions is ± 0.2 eV.

The peak at 284.6 eV was not fit with the characteristic high binding energy asymmetric tail exhibited by graphitic materials. Since small changes in the symmetry of this peak can cause a considerable difference in the amount of oxidized carbon features that can be fitted to the carbon 1s region, the percentage of the carbon 1s photopeak attributed to oxygen and nitrogen functionality in Table IV is skewed to a high value.[70, 78]

Due to the low signal-to-noise ratio of the nitrogen 1s photopeaks, detailed curve-fitting analysis of the nitrogen 1s region was not possible. It was clearly evident, however, that the relative intensity of the portion of the nitrogen 1s photopeak attributed to aromatic amine and imine groups (399.1 eV) increased significantly following ammonia plasma treatment of the AS-4 carbon fibers. The aromatic amine and imine groups are most likely formed on the carbon fiber surface in free radical reactions with the $\bullet NH_2$ and $\bullet NH$ radicals produced in the ammonia plasma. Indeed, due to the reaction sequences and kinetics involved in the plasma decomposition of ammonia, the $\bullet NH_2$ radical is the predominant species available to react with the carbon fiber surface.[40]

The as-received and plasma-treated AS-4 carbon fibers were analyzed at take-off angles of 15° and 90° to determine the relative concentration of species on the outermost surface *versus* deeper within the bulk. The carbon 1s photopeaks of the carbon fibers obtained at take-off angles of 15° and 90° are shown in Figure 10. Based on the shape of the carbon 1s photopeaks and the O/C and N/C ratios, it is evident that the oxygen functional groups created by the air plasma and the nitrogen functional groups introduced by the ammonia plasma are present in greater concentration on the very outermost surface (15°) of the carbon fibers than deeper within the bulk (90°).

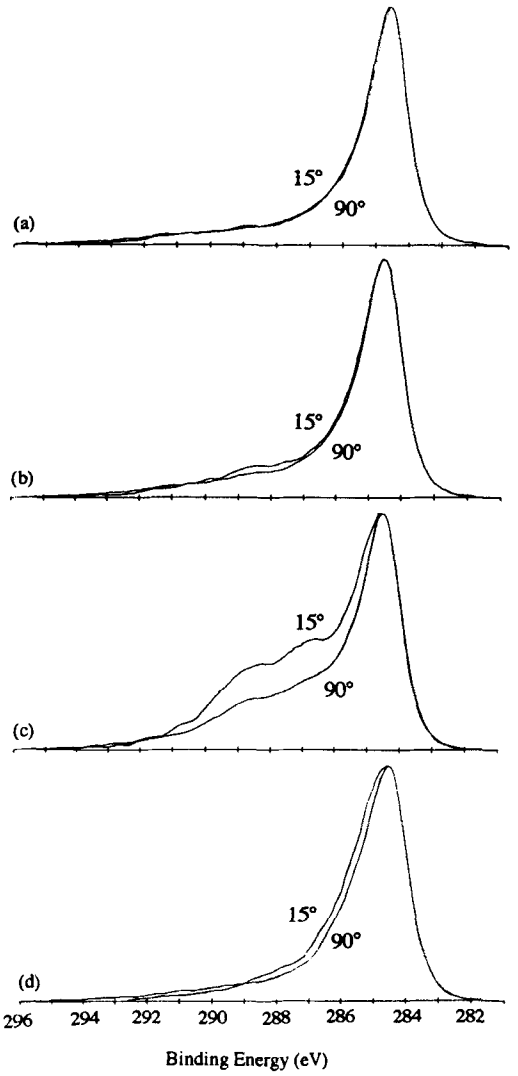

FIGURE 10 Carbon 1s photopeaks obtained at take-off angles of 15° and 90° for (a) as- received AU-4, (b) as received AS-4, (c) 15-sec. air-plasma-treated AS-4, and (d) 1-min. ammonia-plasma-treated AS-4 carbon fibers.

II Topography

At a magnification of 12,500 X, it did not appear that the 15-second air or 1-minute ammonia plasma treatments altered the carbon fiber topography. However, when the fibers were magnified 50,000 X, it was evident that the 15-second air plasma exposure roughened the AS-4 carbon fiber surface. SEM photomicrographs of the as-received and plasma-treated AS-4 carbon fibers magnified 50,000 X are shown in Figure 11. There was no discernible difference between the topography of the as-received AU-4,

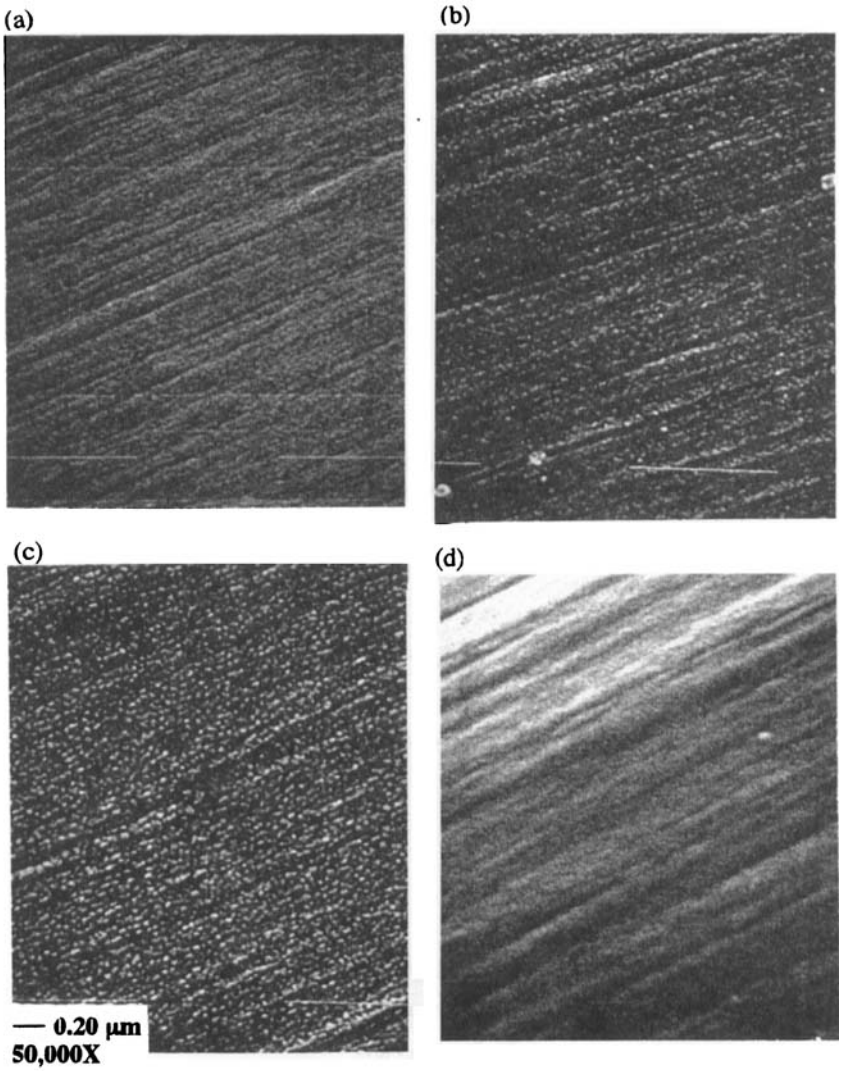

FIGURE 11 SEM photomicrographs of (a) as-received, (b) 15-sec. air plasma, (c) 15-sec. oxygen plasma, and (d) 1-min. ammonia-plasma-treated AS-4 carbon fibers at a magnification of 50,000X.

as-received AS-4 carbon fiber, and 1-minute ammonia-plasma-treated AS-4 carbon fiber at the 50,000 X magnification.

An increase in the carbon fiber surface roughness following oxygen-plasma treatment was observed using scanning electron microscopy by Yuan and coworkers[79] and Jang.[40] Yuan and coworkers saw a change in the carbon fiber topography after a 1-minute oxygen-plasma treatment at a 10,000 X magnification.[79] Jang analyzed the carbon fibers at a 8,000 X magnification and reported that the carbon fiber surface was roughened following a 3-minute oxygen-plasma treatment. In this study, an increase in

surface roughness was seen after only a 15-second air-plasma treatment or a 15-second oxygen-plasma treatment at a 50,000 X magnification. Pattabiraman and coworkers exposed PAN-based carbon fibers and carbon-fiber-reinforced epoxy matrix composites to atomic oxygen, a component of oxygen and air plasmas. They concluded that atomic oxygen is very reactive to the delocalized π electrons in graphitic carbon.[80]

When the carbon fibers were exposed to an ammonia plasma, the surface was not roughened (at a magnification of 50,000 X) and, as shown in Figure 6, there was only a small, initial increase in the concentration of sodium of the fiber surface. Both the SEM and XPS data suggest that the carbon fiber surface was not significantly ablated by the ammonia plasma. Jones and Sammann reported that the basal planes of graphite are inert to the components of an ammonia plasma, but can easily be oxidized by oxygen-containing plasmas.[69, 81]

III Surface Free Energy Analysis

The surface free energies of the carbon fibers obtained using the one-liquid and two-liquid techniques are listed in Table V. In Figure 12, the polar surface free energy and the polar interaction term, obtained using the one-liquid and the two-liquid techniques, respectively, are plotted *versus* the total concentration of oxygen and nitrogen detected on the carbon fiber surface using XPS with a 45° take-off angle. With both techniques, the polar term increased as the concentration of oxygen and nitrogen on the fiber surface was increased. When the one-liquid technique was used, the dispersive surface free energy was relatively constant for all four fibers. However, when the two-liquid technique was used, the dispersive surface free energy varied and the error associated with the dispersive surface free energies of the as-received and ammonia-plasma-treated AS-4 fibers was much larger than with the one-liquid technique.

The variation in the carbon fiber dispersive surface free energy observed in this work with the two-liquid technique has been reported by other researchers. Donnet and coworkers observed a decrease in the dispersive surface free energy component and an increase in the polar component of carbon fibers exposed to an air plasma.[82] Com-

TABLE V
Surface free energy results for the as-received and plasma-treated carbon fibers

FIBER	CARBON FIBER SURFACE FREE ENERGY (mJ/m^2) ($\langle\gamma_S\rangle \pm \sigma_{n-1}$, 7 samples/liquid)						
	one-liquid technique			two-liquid technique			
	γ_S	γ_S^d	γ_S^p	γ_S	γ_S^d	γ_S^p	I_{SF}^p
as-received AU-4	44 ± 3	36 ± 1	8 ± 2	38 ± 3	27 ± 3	11 ± 2	38 ± 2
as-received AS-4	47 ± 2	38 ± 1	9 ± 2	51 ± 7	36 ± 6	15 ± 3	44 ± 3
15-sec. air plasma AS-4	69 ± 2	32 ± 1	37 ± 2	44 ± 2	24 ± 2	20 ± 1	52 ± 1
1-min. NH_3 plasma AS-4	59 ± 3	34 ± 1	26 ± 2	63 ± 8	50 ± 8	13 ± 2	42 ± 3

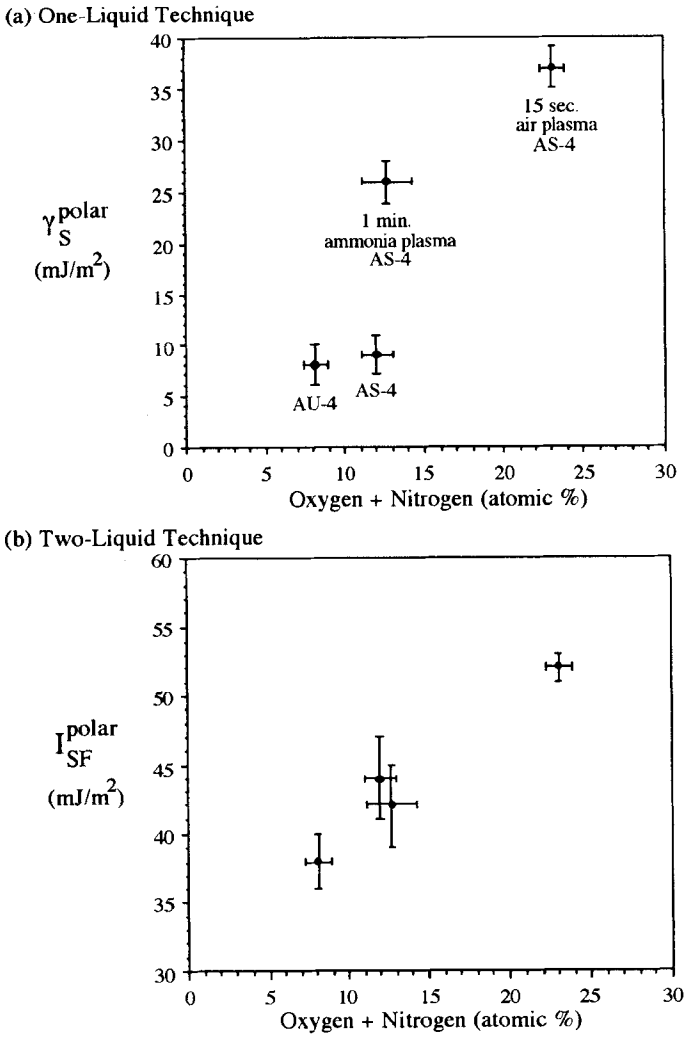

FIGURE 12 (a) Polar surface free energy and (b) polar interaction term plotted *versus* the concentration of oxygen and nitrogen on the surfaces of the as-received and plasma-treated carbon fibers.

merçon and Wightman reported a decrease in the dispersive surface component of carbon fibers following air plasma treatment.[83]

IV Tensile Strength

The tensile strengths of the AU-4 and AS-4 carbon fibers are listed in Table VI. The fiber tensile strength was not affected by plasma treatment, even following the ablative air-plasma treatment. The tensile strength of the as-received AS-4 carbon fibers decreased as the gauge length of the fibers was increased from 0.5 to 2 cm. The tensile

TABLE VI
Average tensile strength of the as-received and plasma-treated carbon fibers

Carbon Fiber	Gauge Length (cm)	Avg. Tensile Strength $\pm \sigma$ (GPa)
as-received AU-4	10	4.4 ± 0.7
as-received AS-4	5	5.3 ± 0.5
as-received AS-4	10	4.5 ± 0.6
as-received AS-4	20	3.9 ± 0.5
15-sec. air plasma AS-4	10	4.2 ± 0.5
1-min. NH_3 plasma AS-4	10	4.4 ± 0.5

strength decreased as the gauge length was increased due to the higher probability of finding a flaw to initiate failure for longer fibers.[63] In this study, gauge lengths from 0.5 to 2 cm were investigated as this was the approximate range of fiber gauge lengths in the microbond experiment.

V Microbond Results

The maximum load measured in the microbond tests with the Matrimid 5292 and BMPPO bismaleimides and the as-received AU-4 and AS-4 carbon fibers is plotted *versus* the fiber embedded length in Figures 13 and 14, respectively. The interfacial shear strength (τ),

$$\tau = \frac{F_{max}}{\text{embedded area}} = \frac{F_{max}}{\pi d L} \tag{10}$$

could not be calculated for the bismaleimide microbond results because the force required to debond the bismaleimide droplets (F_{max}) was independent of the embedded area (L = fiber length embedded in the droplet, d = fiber diameter). There was significant scatter in the data and, in many cases, the carbon fibers failed during the microbond test before sufficient force was applied to debond the bismaleimide droplets.

The scatter in the microbond data may be attributed to testing parameters such as the position of the droplet in the loading fixture, droplet gripping, shape of the meniscus on the polymer droplet, and faulty measurement of the fiber diameter and embedded length. In addition, variations in the chemical, physical or morphological nature of the fiber along its length may affect the carbon fiber/polymer adhesion.[1] Figure 15 is a schematic illustration which demonstrates a number of the parameters involved in the microbond test.

When the debonded bismaleimide droplets were examined using the scanning electron microscope, a "crown" of polymer was seen on the fiber where the bismaleimide droplet was originally located. Scanning electron photomicrographs of a typical debonded bismaleimide droplet is shown in Figure 16. During the debonding process,

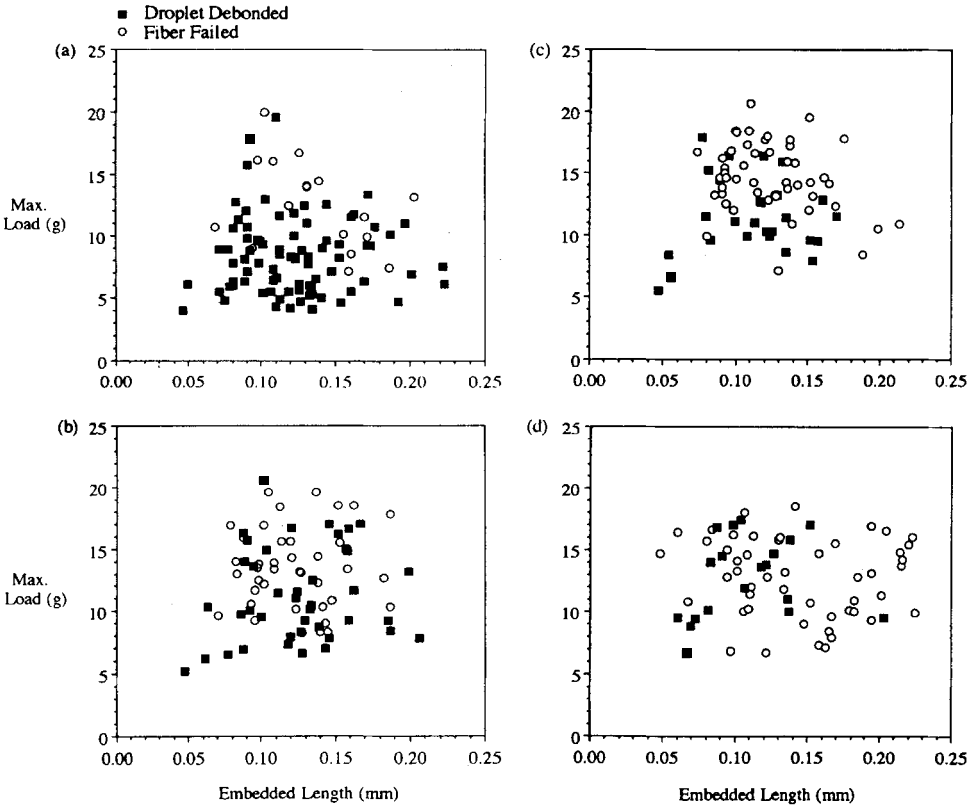

FIGURE 13 Maximum load measured in the microbond experiments with the Matrimid 5292 bismaleimide and (a) as-received AU-4, (b) as-received AS-4, (c) 15-sec. air-plasma-treated AS-4, and (d) 1-min. ammonia-plasma-treated AS-4 carbon fibers as a function of the fiber embedded length.

the meniscus at the top of the bismaleimide droplet failed. The existence of the polymer crown shows that the bismaleimide was well bonded to the fiber surface. If "good" adhesion did not exist between the bismaleimide droplet and the fiber, the entire droplet would have simply slid down the fiber when load was applied and the meniscus would not have failed.

The scanning electron photomicrographs of the bismaleimide droplets in Figure 17 reveal that the shape of the meniscus played a role in the data scatter. The bismaleimide meniscus, shown in Figure 17 (a), is not axisymmetric. When the meniscus is not axisymmetric, the shearing plates do not contact both sides of the bismaleimide droplet simultaneously and the droplet is loaded in a skewed, off-axis direction. In Figure 17(b), the bismaleimide meniscus extends down the length of the fiber. Interfacial failure initiated above the shearing plates, creating a much greater embedded length than was measured with the optical microscope prior to microbond testing.

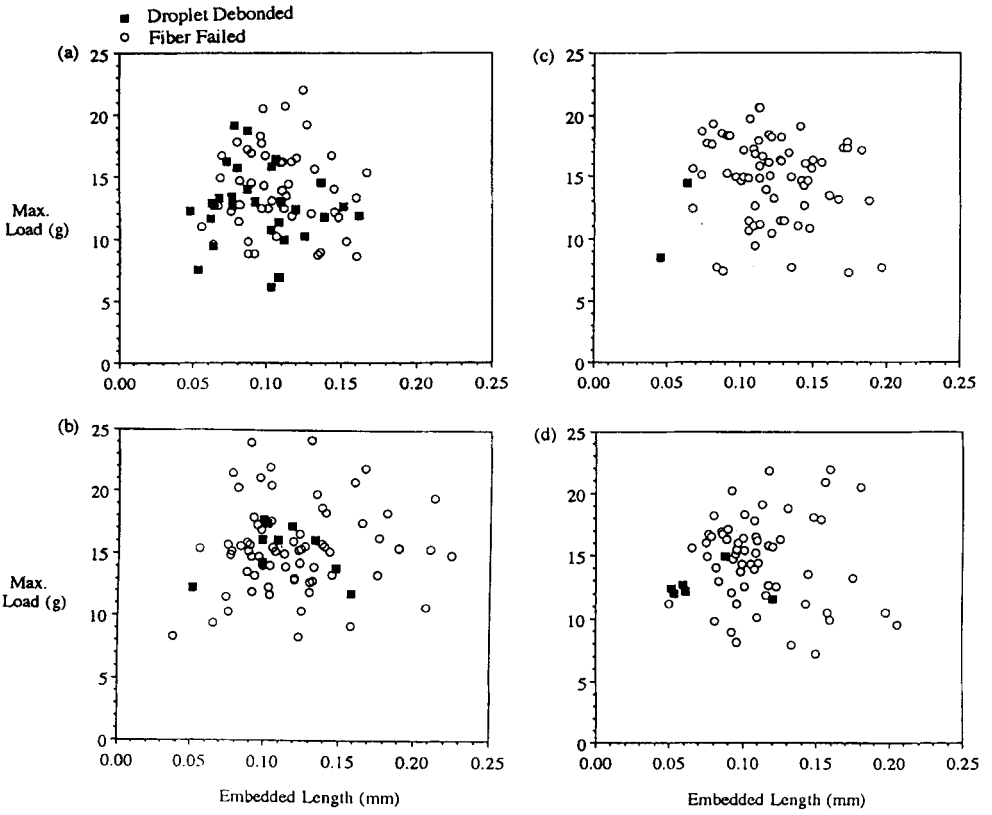

FIGURE 14 Maximum load measured in the microbond experiments with the BMPPO bismaleimide and (a) as-received AU-4, (b) as-received AS-4, (c) 15-sec. air-plasma-treated AS-4, and (d) 1-min. ammonia-plasma-treated AS-4 carbon fibers as a function of the fiber embedded length.

Examples of the load *versus* displacement plots obtained in typical microbond experiments with carbon fibers and bismaleimide droplets are shown in Figure 18. In Figure 18(a), the load rose linearly from zero as the fiber was strained and dropped when the bismaleimide droplet debonded. A second linear rise was then observed up to a second peak load. A plateau where the load was randomly displaced about a mean followed the second peak load. The maximum load measured was recorded as the debond load. With a few of the bismaleimide microbond samples, a load *versus* displacement curve such as that in Figure 18(b) was obtained. In this case, it appears that a crack initiated but did not propagate down the entire interface. An additional load was required to debond the bismaleimide droplet completely from the fiber. An example of the load *versus* displacement curves obtained when the carbon fiber failed during microbond testing is shown in Figure 18(c).

When the carbon fiber failed during a microbond test, the microbond specimen fell and was collected on a piece of adhesive tape positioned below the shearing plates. In

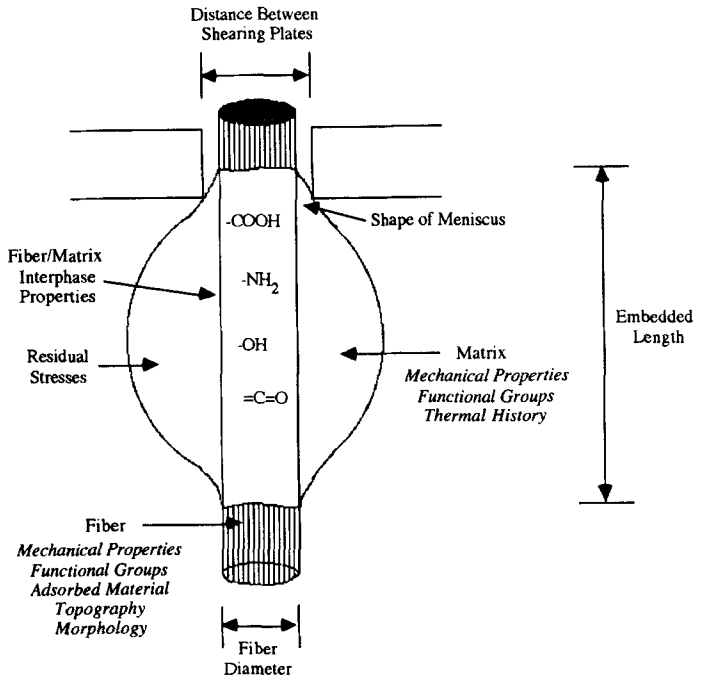

FIGURE 15 Parameters involved in the microbond single-fiber pull-out test.

many cases, the carbon fiber failed within the bismaleimide droplet, as shown in Figure 19. The bismaleimide meniscus failed, a crack propagated for some length down the fiber/matrix interface and then, at some point, the carbon fiber failed within the bismaleimide droplet. There is a hole in the top of the droplet where the upper portion of the broken carbon fiber pulled out of the bismaleimide resin. The lower portion of the failed fiber extends from the bottom of the droplet.

Figure 20 is a bar chart which shows the percentage of the bismaleimide droplets ($L \leq 100\ \mu m$) which were successfully debonded without fiber failure during microbond testing with the as-received AU-4 and AS-4 fibers and the 1-minute ammonia-plasma and 15-second air-plasma-treated AS-4 fibers. Only the microbond data for the bismaleimide droplets with embedded lengths less than 100 μm were used to calculate the percentage of droplets successfully debonded, due to the increased probability of fiber failure as the embedded length increased. The number of bismaleimide droplets which were successfully debonded without failure of the carbon fiber decreased as the carbon fiber/bismaleimide interfacial strength increased to a point where the fiber strength was exceeded during microbond testing. Since the debond load was independent of the fiber embedded length and the interfacial shear strength could not be determined, the average debond load and the percent occurrence of fiber failures were used as measures of the adhesion between the bismaleimide resins and the carbon fibers.

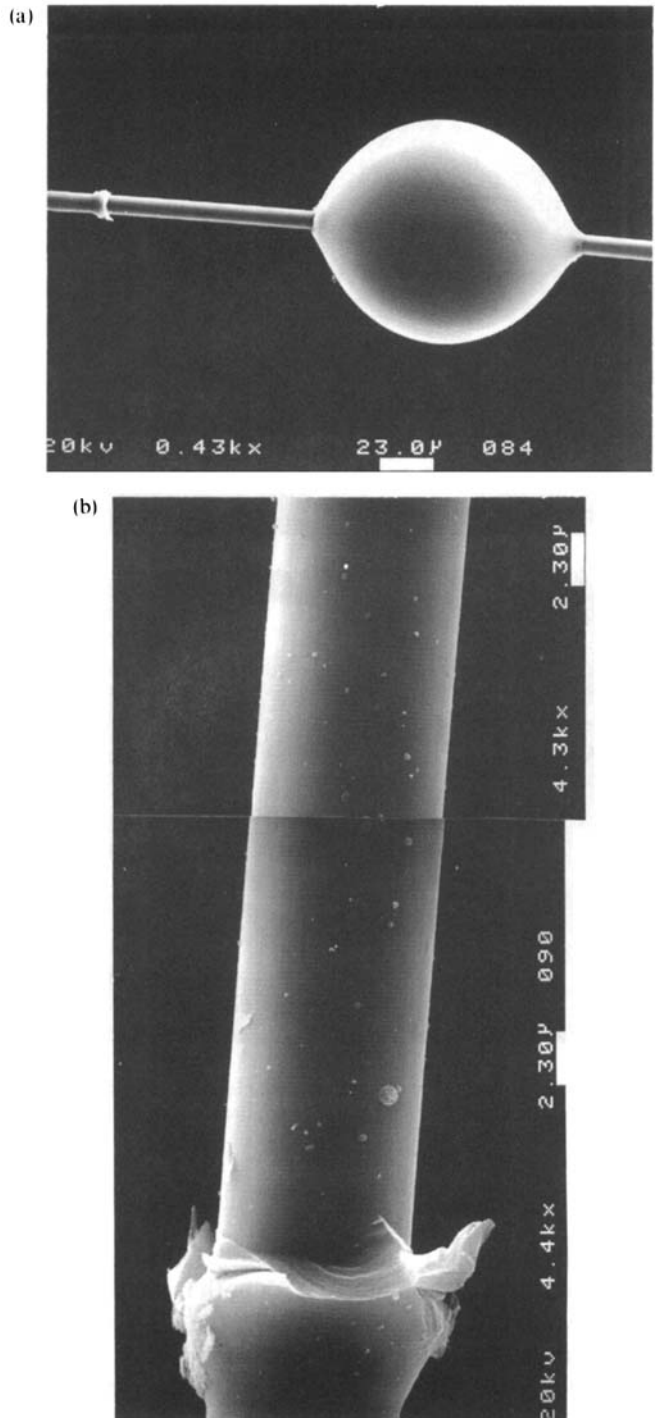

FIGURE 16 SEM photomicrographs at (a) 430X and (b) 4,400X of a BMPPO bismaleimide droplet which debonded from an as-received AS-4 carbon fiber.

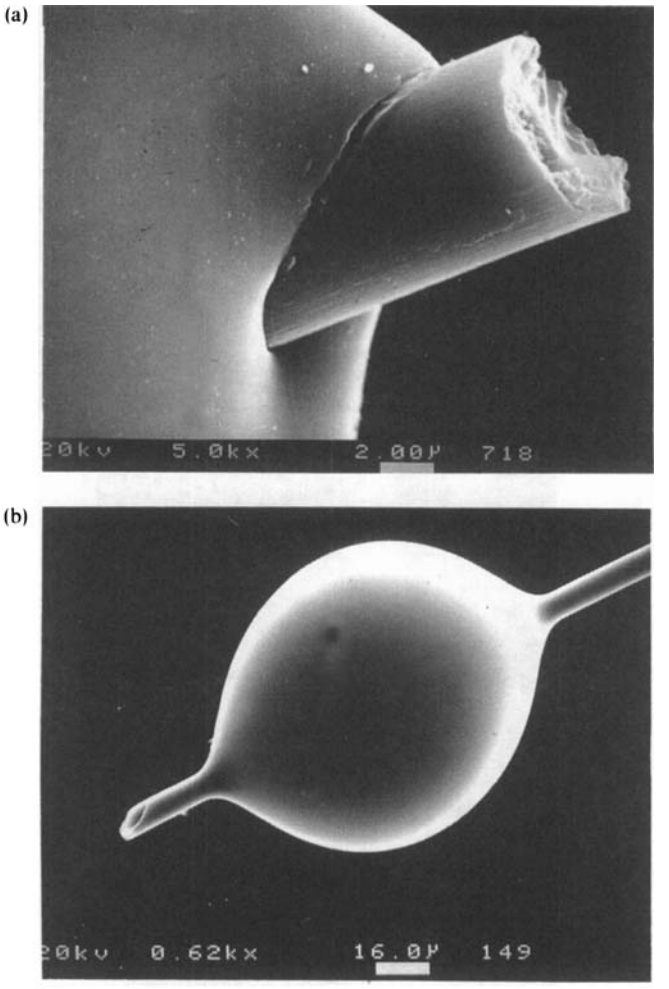

FIGURE 17 SEM photomicrographs of carbon fiber/bismaleimide microbond specimens following testing with (a) a nonsymmetric meniscus (5,000X) and (b) an embedded length greater than that measured using optical microscopy prior to testing (620X).

Figure 21 shows the average load required to debond the bismaleimide droplets from the as-received AU-4 and AS-4 carbon fibers. With both bismaleimides, a greater load was required to fail the interface with the surface-treated AS-4 carbon fiber than with the untreated AU-4 carbon fiber. In addition, a greater percentage of the AS-4 fibers failed during microbond testing before sufficient load could be applied to debond the bismaleimide droplet from the fiber.

XPS and wetting analyses showed that the proprietary commercial surface treatment used to convert the AU-4 to the AS-4 carbon fiber increased both the fiber surface free energy and the concentration of oxygen and nitrogen on the fiber surface. No

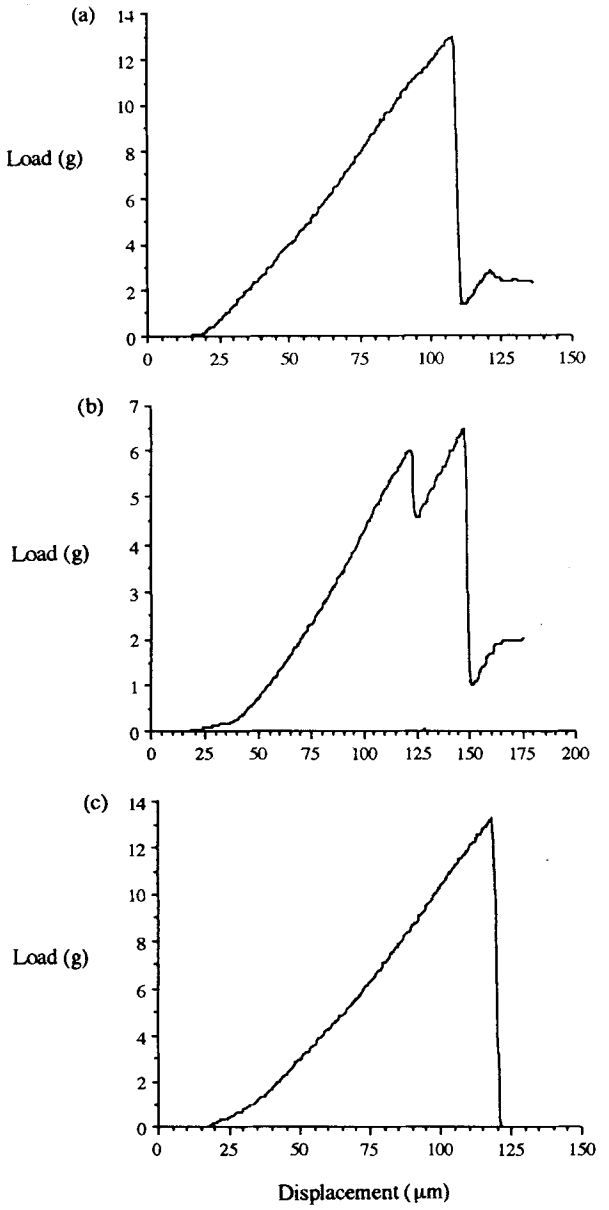

FIGURE 18 Load *versus* displacement curves obtained when (a&b) the bismaleimide droplet debonded from the carbon fiber and (c) the carbon fiber failed during the microbond test.

change in the surface topography was evident by SEM at a magnification of 50,000 X. This suggests that the AS-4 carbon fiber/bismaleimide adhesion was greater than the AU-4 carbon fiber/bismaleimide adhesion and.that the enhanced adhesion to the AS-4 carbon fiber may be due to an increase in the fiber wettability and/or specific chemical

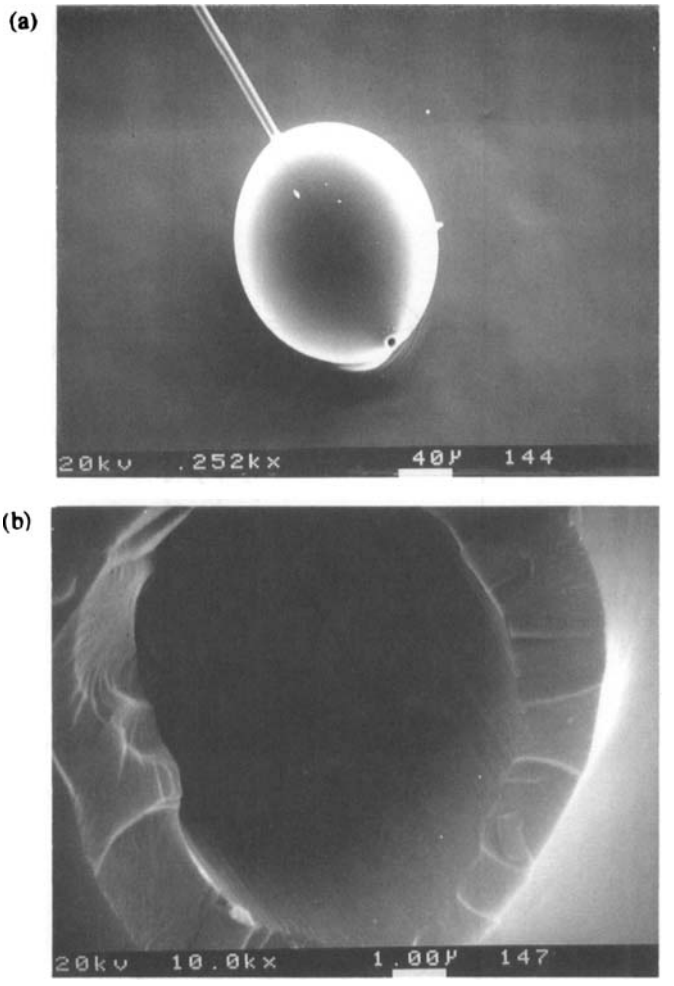

FIGURE 19 SEM photomicrographs at (a) 252X and (b) 10,000X of a carbon fiber/bismaleimide microbond specimen which exhibited fiber failure within the bismaleimide droplet during microbond testing.

interactions between the bismaleimide resins and active sites on the carbon fiber surface. Drzal and coworkers have also suggested that inferior adhesion to AU-4 carbon fibers may be due to a weakly-bound layer on the AU-4 carbon fiber surface.[4]

The microbond data also suggest that both the Matrimid 5292 bismaleimide and the BMPPO bismaleimide adhered better to the air-plasma-treated AS-4 carbon fibers than to the as-received AS-4 carbon fibers. The 15-second air-plasma treatment roughened the fiber surface, increased the concentration of oxygen and nitrogen on the fiber surface, and increased the carbon fiber surface free energy. Therefore, superior adhesion of the bismaleimide resins to the air-plasma-treated carbon fibers may be due mechanical interlocking effects, improved fiber wettability, and/or an increase in the

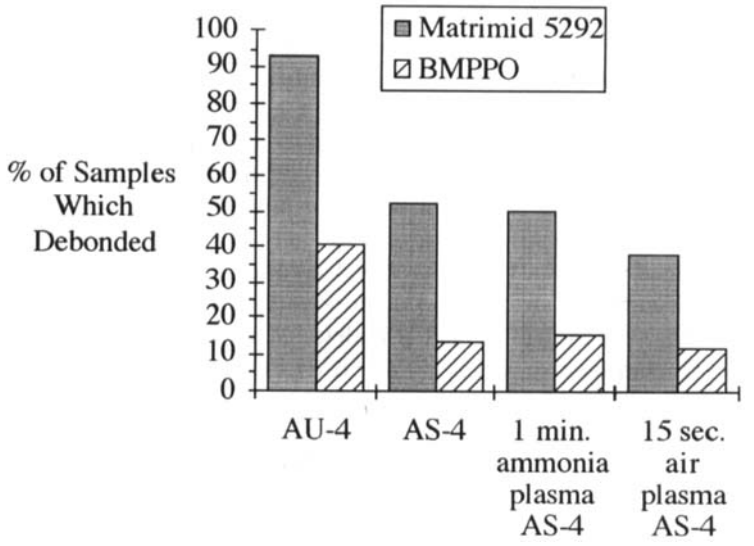

FIGURE 20 Percentage of bismaleimide droplets which debonded during microbond testing with the as-received and plasma-treated carbon fibers.

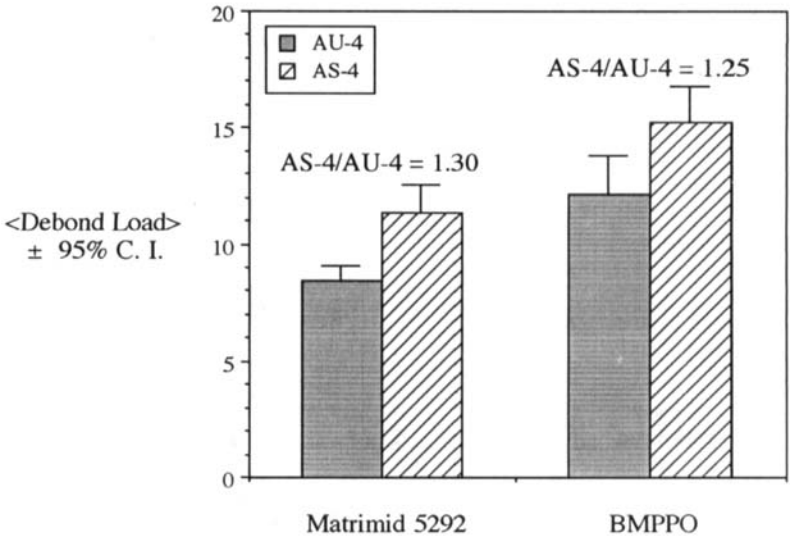

FIGURE 21 Average load at which the Matrimid 5292 and BMPPO bismaleimide droplets debonded from the as-received AU-4 and AS-4 carbon fibers.

number of active sites on the fiber surface for specific chemical interactions with the bismaleimide resin.

The percentage of the bismaleimide droplets which were successfully debonded without fiber failure was not significantly different for the as-received and the ammo-

nia-plasma-treated AS-4 carbon fibers even though the ammonia plasma significantly increased the concentration of nitrogen on the fiber surface. It was postulated by Jang that the amine groups created on the carbon fiber surface in an ammonia plasma improve bismaleimide adhesion by undergoing nucleophilic Michael additions with the maleimide double bond.[40] The effect of nitrogen-containing functional groups on carbon fiber-bismaleimide adhesion was not apparent in this work. However, since most of the AS-4 and plasma-treated carbon fibers failed during microbond testing, the carbon fiber/bismaleimide adhesion results are skewed to lower values than would have been obtained if 100% of the microbond samples had debonded.

The data in Figures 20 and 21 also demonstrate that the BMPPO bismaleimide adhered better than the Matrimid 5292 bismaleimide to all four carbon fibers. This may be because the compressive forces in the BMPPO droplets are greater that the compressive forces in the Matrimid droplets. Compressive residual stresses develop in the bismaleimide droplets due to the bismaleimide cure reaction and due to the fact that upon cooling from the cure temperature to ambient temperature, the fiber and the bismaleimide droplet do not contract equally.

After the bismaleimide droplet debonded in the microbond test, the load fell to zero and then rose linearly to a second peak load (see Fig. 17(a)). This second peak load was taken as a relative comparison of the load required to overcome the compressive forces which physically lock the fiber within the droplet.[34] When the droplet debonded, the strain energy in the fiber relaxed, causing a sudden decrease in the fiber length and a sudden increase in the fiber diameter due to the Poisson's ratio of the fiber. When the fiber diameter returned to its original value, the fiber resumed contact with the internal

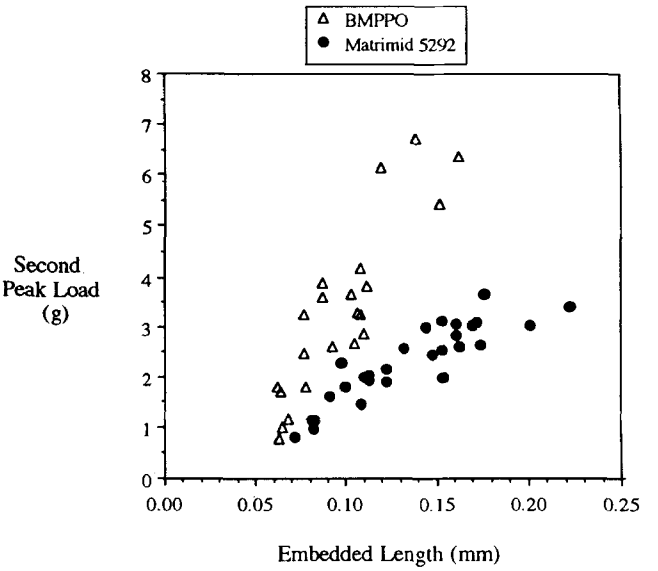

FIGURE 22 Second peak load measured for the BMPPO and Matrimid 5292 bismaleimide droplets as a function of the fiber embedded length.

surface of the bismaleimide droplet. Chemical bonding no longer existed between the fiber and the droplet and the fiber was now physically locked in the droplet.

The second peak load measured for the BMPPO and the Matrimid 5292 bismaleimide droplets is plotted *versus* the fiber embedded length in Figure 22. With both bismaleimides, the second peak load increased with the embedded length. However, the second peak load was greater in the BMPPO bismaleimide droplets than in the Matrimid 5292 bismaleimide droplets. Both the modulus and the linear expansion coefficient of the BMPPO and the Matrimid 5292 bismaleimides, material parameters which could contribute to the difference in the microbond data, were measured and determined to be, within experimental error, equivalent for the two different bismaleimides. While the residual stresses in the bismaleimide droplets do physically "clamp" the droplets on the fibers, the effect of fiber surface treatment on bismaleimide adhesion demonstrates that fiber surface properties also play an important role in carbon fiber/bismaleimide adhesion.

SUMMARY

A technique was developed to cure bismaleimide drops around singe carbon fibers for microbond testing. However, use of the microbond test to evaluate the carbon fiber/bismaleimide interface was limited by the strength of the fibers. Even though the length of the carbon fibers embedded in the bismaleimide drops ranged from only 40 to 200 μm, a large proportion of the fibers failed during the microbond test. The percentage of carbon fibers which failed during microbond testing, a measure of the carbon fiber/bismaleimide adhesion, was affected by both the carbon fiber surface properties and the compressive residual stresses in the bismaleimide droplets.

The carbon fiber adhesion of both a novel phosphorus-containing bismaleimide and a commercially-available bismaleimide improved when the fibers were surface treated prior to bonding. Both bismaleimides adhered better to surface-treated AS-4 carbon fibers than to untreated AU-4 carbon fibers. Superior adhesion of the bismaleimide resins to the surface-treated carbon fibers may be attributed to an increase in the fiber surface free energy and wettability, removal of a weakly-bound fiber surface layer, and an increase in the number of active sites on the fiber surface for specific chemical interactions with the polymer matrix.

Acknowledgements

The authors extend their gratitude to Mr. Steve McCartney for taking the SEM photomicrographs of the carbon fibers, Mr. Frank Cromer for assisting with the surface analysis, and Dr. Pascal Commerçon for designing the microbond test equipment. This research was funded by the National Science Foundation Science and Technology Center for High Performance Polymeric Adhesives and Composites under contract DMR-8809714.

References

1. P. J. Herrera-Franco and L. T. Drzal, *Composites* **23**(1), 2 (1992).
2. L. T. Drzal in *Controlled Interphases in Composite Materials*, H. Ishida, Ed. (Elsevier Science, New York, 1990), p. 309.

3. M. Nardin and J. Schultz, in *Proceedings of NATO-ASI on The Interfacial ınteractions in Polymeric Composites*, G. A. Kovali, Ed. (Kluwer Acad. Publ., Dordrecht, 1993), pp. 95–105.
4. L. T. Drzal, M. J. Rich and P. F. Lloyd, *J. Adhesion* **16,** (1982).
5. J. P. Favre and D. Jaques, *J. Mater. Sci.* **25,** 1373 (1990).
6. V. Rao and L. T. Drzal, *Polym. Comp.* **12** (1), 48 (1991).
7. J. Schultz, L. Lavielle and C. Martin, *J. Adhesion* **23,** 45 (1987).
8. L. T. Drzal, M. J. Rich, M. F. Koenig and P. F. Lloyd, *J. Adhesion* **16,** 133 (1983).
9. W. D. Bascom and R. M. Jensen, *J. Adhesion* **19,** 219 (1986).
10. S. M. Lee and S. Holguin, *J. Adhesion* **31,** 91 (1990).
11. A. T. DiBenedetto, *Comp. Sci. Technol.* **42,** 103 (1991).
12. L. T. Drzal, M. C. Waterbury and M. Madhukar, *37th Int. SAMPE Symp.* (1992), p. 770.
13. J. C. Figueroa, T. E. Carney, L. S. Schadler and C. Laird, *Comp. Sci. Technol.* **42,** 77 (1991).
14. X. S. Bian, L. Ambrosio, J. M. Kenny, L. Nicolais, E. Occhiello, M. Morra, F. Garbassi and A. T. Dibenedetto, *J. Adhesion Sci. Technol.* **5** (5), 377 (1991).
15. G. Merle and M. Xie, *Comp. Sci. Technol.* **40,** 19 (1991).
16. V. Rao and L. T. Drzal, *J. Adhesion* **37,** 83 (1992).
17. W. G. Pitt, J. E. Lakenan and A. B. Strong, *J. Appl. Polym. Sci.* **48** (5), 845 (1993).
18. W. A. Frazer,F. H. Ancker, A. T. DiBenedetto and B. Elbirli, *Polymer Composites* **4,** 238 (1983).
19. V. Rao, P. Herrera-Franco, A. D. Ozzello and L. T. Drzal, *J. Adhesion* **34,** 65 (1991).
20. I. Verpoest, M. Desaeger and R. Keunings in *Controlled Interphases in Composite Materials*, H. Ishida, Ed. (Elsevier Science, New York, 1990), p. 653.
21. A. N. Netravali, D. Stone, S. Ruoff and L. T. T. Topoleski, *Compos. Sci. Technol.* **34,** 289 (1989).
22. E. J. H. Chen and J. C. Young, *Comp. Sci. Technol* **42,** 189 (1991).
23. U. Gaur and B. Miller, *Comp. Sci. Technol.* **34,** 35 (1989).
24. B. Miller, P. Muri and L. Rebenfeld, *Compos. Sci. Technol.* **18,** 17 (1987).
25. L. S. Penn and B. Jutis, *J. Adhesion* **30,** 67 (1989).
26. C. T. Chou and L. S. Penn, *J. Adhesion* **36,** 125 (1991).
27. K. Küpper and P. Schwartz, *J. Adhesion Sci. Technol.* **5**(2), 165 (1991).
28. U. Gaur, G. Desio and B. Miller, *Plastics Engineering* (Oct. 1989), p. 43.
29. B. Miller, U. Gaur and D. E. Hirt, *Comp. Sci. Technol.* **42,** 207 (1991).
30. S. L. Chuang and N. J. Chu, *J. Appl. Polym. Sci.* **41,** 373 (1990).
31. V. Rao and L. T. Drzal, *J. Adhesion* **35,** 245 (1991).
32. P. S. Chua and M. R. Piggott, *Comp. Sci. Technol.* **22,** 107 (1985).
33. P. S. Chua and M. R. Piggott, *Comp. Sci. Technol.* **22,** 185 (1985).
34. P. Marshall and J. Price, *Composites* **22** (1), 53 (1991).
35. D. N. Hild and P. Schwartz, *J. Adhesion Sci. Technol.* **6** (8), 897 (1992).
36. M. J. Pikethly and J. B. Doble, *Composites* **21** (5), 389 (1990).
37. Y. Qiu and P. Schwartz, *J. Adhesion Sci. Technol.* **5** (9), 741 (1991).
38. C. Galiotis, *Compos. Sci. Technol.* **42,** 125 (1991).
39. A. I. Sviridenok, T. K. Sirotina and E. V. Pisanova, *J. Adhesion Sci. Technol.* **5,** 229 (1991).
40. B. Z. Jang, *Comp. Sci. Technol.* **44,** 333 (1992).
41. T. R. King, D. F. Adams, D. A. Buttry, *Composites* **22** (5), 380 (1991).
42. W. Wenig and T. Schöller, *Colloid Polym. Sci.* **269,** 1212 (1991).
43. A. G. Evans, F. W. Zok and J. Davis, *Comp. Sci. Technol.* **42,** 3 (1991).
44. S. M Lee, *Comp. Sci. Technol.* **43,** 317 (1992).
45. H. W. Rhee and J. P. Bell, *Polymer Composites*, **12** (4), 213 (1991).
46. H. Stenzenberger, M. Herzoq, W. Romer and R. Scheiblich, *30th Nat. SAMPE Symposium*, **30** (1985),p. 1568.
47. H. Stenzenberger in *Polyimides*, D. Wilson, H. D. Stenzenberger and P. M. Hergenrother, Eds. (Chapman & Hall, New York, 1990), p. 79.
48. H. Stenzenberger, in *Structural Adhesives: Developments in Resins and Primers*, A. J. Kinloch, Ed. (Elsevier Applied Science Publishers, New York, 1986), p. 77.
49. B. Z. Jang, *Compos. Sci. Technol.* **44,** 333 (1992).
50. S. P. Wilkinson, PhD. Dissertation, Virginia Polytechnic Institute and State University, Blacksburg, Virginia 24061 USA (1991).
51. R. E. Allred and L. A. Harrah, *34th Int. SAMPE Symp.* **34,** 2559 (1989).
52. S. M. Lee and S. Holguin, *J. Adhesion* **31,** 91 (1990).
53. P. A. Wood, G. D. Lyle, A. Gungor, C. D. Smith and J. E. McGrath, *36th Int. SAMPE Symposium* **36,** 1355 (1991).
54. C. D. Smith, H. Grubbs, H. F. Webster, A. Gungor, J. P. Wightman and J. E. McGrath, *High Perf. Polym.* 3(4), 211 (1991).

55. I. K. Varma, G. Fohlen and J. A. Parker, US Patent 4276344, 1981.
56. J. E. Mark, H. R. Allcock and R. West, *Inorganic Polymers* (Prentice Hall, Edgewood Cliffs, New Jersey, 1992), p. 237.
57. C. Jones, *Compos. Sci. Technol.* **42,** 275 (1991).
58. A. W. Adamson, *Physical Chemistry of Surfaces*, 5th ed. (Wiley-Interscience, New York, 1990).
59. F. M. Fowkes in *Treatise on Adhesion and Adhesives- Vol. 1*, R. L. Patrick, Ed. (Marcel Dekker, New York, 1967), p. 325.
60. D. K. Owens and R. C. Wendt, *J. Appl. Polym. Sci.* **13,** 1741 (1969).
61. P. J. Dynes and D. H. Kaelble, *J. Adhesion* **6,** 195 (1974).
62. D. H. Kaelble and P. J. Dynes, *J. Adhesion* **6,** 239 (1974).
63. J. B. Donnet and R. C. Bansal, *Carbon Fibers*, 2nd ed. (Marcel Dekker, New York, 1990).
64. J. Schultz, C. Cazeneuve, M. E. R. Shanahan and J. B. Donnet, *J. Adhesion* **12,** 221 (1981).
65. D. H. Kaelble and K. C. Uy, *J. Adhesion* **2,** 50 (1970).
66. F. M. Fowkes, *J. Adhesion Sci. Technol.* **1,** 7 (1987).
67. C. P. Beetz, Jr., *Fiber Science & Technology* **16,** 45 (1982).
68. A. K. Gupta, D. K. Paliwal and P. Bajaj, *J. Macromol. Sci.-Rev. Macromol. Chem. Phys.* **C31,** (1991).
69. C. Jones and E. Sammann, *Carbon* **28,** 509 (1990).
70. E. Desimoni, G. I. Casella, A. Morone and A. M. Salvi, *Surf. Interf. Analysis* **15,** 627 (1990).
71. E. Desimoni, G. I. Casella, T. R. I. Calaldi, A. M. Salvi, T. Rotunno, E. DiCroce, *Surf. Interf. Analysis* **18,** 623 (1992).
72. G. Beamson and D. Briggs, *High Resolution XPS of Organic Polymers* (John Wiley & Sons, New York, 1992).
73. C. Kozlowski and P. M. A. Sherwood, *Carbon* **25,** 751 (1987).
74. A. Proctor and P. M. A. Sherwood, *J. Electron Spectrosc. Related Phenom.* **27,** 39 (1982).
75. C. Kozlowski and P. M. A. Sherwood, *J. Chem. Soc., Faraday Trans.* **80,** 2099 (1984).
76. C. Kozlowski and P. M. A. Sherwood, *J. Chem. Soc., Faraday Trans.* **81,** 2745 (1987).
77. Y. Xie and P. M. A. Sherwood, *Chem. Mater.* **1,** 427 (1989).
78. Y. Nakayama, F. Soeda and A. Ishitani, *Carbon* **28,** 21 (1990).
79. L. Y. Yuan, C. S. Chen, S. S. Shyu and J. Y. Lai, *Compos. Sci. Technol.* **45,** 1 (1992).
80. P. Pattabiraman, N. M. Rodriguez, B. Z. Jang and R. T. K. Baker, *Carbon* **28** (6), 867 (1990).
81. C. Jones and E. Sammann, *Carbon* **28,** 515 (1990).
82. J. B. Donnet, M. Brendle, T. L. Dhami and O. P. Bahl, *Carbon* **24,** 757 (1986).
83. P. Commerçon and J. P. Wightman, *J. Adhesion* **38,** 55 (1992).